

Temporal network-based analysis of oceanic flow with applications to marine ecology

Kishor Acharya^{1†}, Javier Aguilar^{2†}, Lorenzo Dall’Amico^{3†}, Kyriacos Nicolaou^{4†}, Johnny Tong^{5†}, Enrico Ser-Giacomi^{2*},

1 University of Luxembourg, Luxembourg

2 IFISC, Spain

3 ISI Foundation, Turin, Italy

4 Utrecht University, The Netherlands

5 Technical University of Munich, Germany

† Authors contributed equally

* Corresponding author: enrico.sergiacomi@gmail.com

Abstract

In this report we present the work carried out during the Complexity72h workshop, held at IFISC in Palma de Mallorca, Spain, 26-30 June 2023. We describe a temporal network-theoretic approach to study fluid flows with applications to marine ecology. The network representation is derived from the Lagrangian fluid dynamics and represents fluid transportation between patches of the sea. It is a directed, weighted and time-dependent network. This approach enables us to use advanced network-theoretic tools for analysis and modeling. A common approximation adopted in the literature consists in using an aggregated time-independent network representation of the fluid flow. In this report we focus in particular on the role played by the temporal component and to the information loss related to neglecting that dimension and inspect the role played by seasonal or long time-period variations. We conduct an analysis of basic network features of the aggregated and temporal graphs, we analyze their community structure and we model population dynamics of marine lives driven by the flow. Ultimately, we determine that time-independent approximations can effectively represent long-term transportation evolution spanning multiple years. On the other hand, to show seasonal variations in a year, it is necessary to incorporate explicit time-dependence in the transport matrix to account for seasonality.

Introduction

The marine ecosystems play an important role in our society, influencing, for instance, land ecosystems [1], economics [2], as well as public health [3]. The structure and function of marine ecosystems respond drastically to seasonal changes and climatic variations [4]. Environmental fluctuations can thus affect the plankton community structure, as well as the spatial distribution of fish and invertebrates, the recruitment success of pelagic fish and even the mortality of birds and mammals [5]. Marine ecosystems are embedded in patches of water that are continuously moving, stretching, and diluting. These processes drive inhomogeneities in a wide span of scales and global patterns of marine population dynamics are majorly determined by the dispersion of oceanic currents, with implications for the integrated ecosystem properties [6]. Due to the intrinsic challenges

of researching the marine environment and the limited availability of spatial data, it is hard to track the marine population directly. However, recent advances of satellite imaging and hydrodynamic modelling data made possible the open access to oceanic flow patterns [7]. One of the approaches used to characterize flow-driven dispersal of oceanic currents and propagules is to simulate the flow of synthetic particles using the hydrodynamic data [8]. Lagrangian particle trajectories can then be translated into transport matrices, that can be interpreted as weighted, temporal, directed networks. This allows one to rigorously investigate maritime flows with graph theoretical tools [9].

We here consider a snapshots temporal network [10], collected in the Mediterranean sea and corresponding to one-month windows of the same year (2002) and to the same month (July) across 10 years (from 2002 to 2011). A common approach to deal with these data (see for instance [9]) is to consider a time-aggregated network obtained by averaging all the snapshots across the years. To the best of our knowledge, the explicit time dependence of these networks has not been considered in previous studies and is the focus of this report. By exploiting network-theoretic techniques, we quantify the differences between the temporal and aggregated graphs in terms of link density, degree and weight distributions, and community structure. These metrics show the topological structure of the transport networks and allow us to qualitatively evaluate how physical behaviors such as dispersion and mixing depend on seasons and climate. Time-independent networks exhibit significant differences in the distribution of degrees and weights compared to the time-dependent instances across all datasets. However, notable changes in communities are observed only when considering snapshots within the same year, while minimal evolution is observed when examining the same month across different years. This suggests that structural changes are primarily induced by seasonal effects.

In order to assess the effect of time-dependent transportation in marine populations, we formulate the marine population dynamics in with two advection-reaction-like models on top of the flow network. We compare the results obtained when using the temporal networks against the aggregated networks to characterize how the oceanic flow seasonally and climatically affect the population distribution of marine lives and its robustness to regulate the population against abrupt events. We find that the time-independent description tends to generate smoother patterns compared to the ones obtained with the faithful time-dependent representation.

While our results were primarily conceived to apply to marine sedentary populations, whose dispersal is mediated by marine currents, our conclusions may potentially relate to how air-borne dispersal of sedentary terrestrial populations is evaluated as well.

Methods

This section delineates the methodology adopted to obtain the main results and provides a description of the data our analysis relies upon. We first describe how the temporal network is obtained from the original data. We then delineate some basics of community detection used to study the meso-scale structure of the so-obtained network and we describe a biophysical model for population dynamics of marine organisms passively transported by the currents.

Network construction

We exploit the data taken from the Mediterranean Forecasting System (MFS) based on NEMO-OPA (Nucleus for European Modelling of the Ocean-PArellelis, version 3.2 [7]). This data-assimilative operational model has been implemented in the Mediterranean at

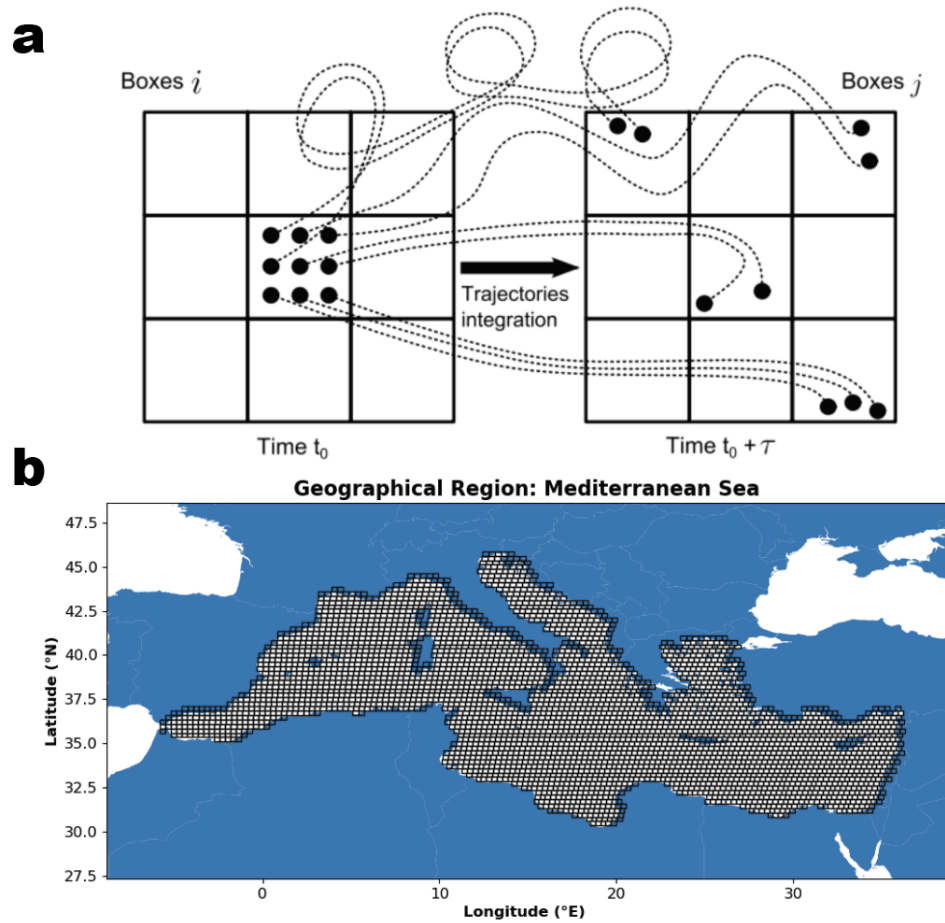


Figure 1. Transport matrix construction from the hydrodynamical data In (a), transport matrix is constructed from tracer’s advection following Eq. (1). In (b), the Mediterranean sea is discretized into $N = 3270$ equal-area boxes and apply the pipeline as in (a) to obtain the transport matrices over 12 months.

$1/16^\circ$ degree horizontal regular resolution and 72 unevenly spaced verticals levels [11]. We use the physics reanalysis products for years spanning 2002-2011 downloaded from Marine Copernicus website marine.copernicus.eu.

Following the procedure described in [9], we discretize the Mediterranean basin on a grid of 8196 patches of 0.25° resolution. We create a network, representing each patch as a node and we add directed edges encoding the exchange of fluid that moved from one patch to the another in a given time interval. Each edge has an associated weight proportional to the amount of fluid transported. This quantity is obtained from a Lagrangian dynamics by following trajectories of ideal fluid particles and keeping record of their initial and final positions (i.e. starting and ending nodes) during the time interval considered. More specifically, we integrate for a fixed time τ the equation of motion for each particle, from the initial condition \mathbf{x}_0 at time t_0 until the final position at $t_0 + \tau$, using a velocity field $\mathbf{v}(\mathbf{x}, t)$, defining the flow map $\Phi_{t_0}^\tau$:

$$\mathbf{x}(t_0 + \tau) = \Phi_{t_0}^\tau(\mathbf{x}_0),$$

which determines the motion of single fluid particles. By considering the action of the flow map on all the points contained in a fluid region A we define the action of

$\Phi_{t_0}^\tau$ on whole sets: $A(t_0 + \tau) = \Phi_{t_0}^\tau(A(t_0))$. We then place 100 particles per node to initialize the system. In practice, trajectories are simulated by integrating the velocity field, bilinearly interpolated using a Runge-Kutta 4 algorithm with a time step of $0.3 h$, fulfilling the Courant-Friedrichs-Lewy condition [12]. We assume that the transport we deal with is primarily in two dimensions and neglect transport in the vertical dimension. In particular, we use the MFS horizontal velocity fields of the 3rd and 17th vertical levels, which correspond to about $12 m$ for the shallow coastal habitat and $102 m$ for the neritic shelf habitat, respectively.

Applying the flow map to the discrete boxes, we have an estimation of the flow among each pair of nodes. Given the collection of boxes $\{B_i, i = 1, \dots, N\}$, we represent the transport between them by the discrete version of the Perron-Frobenius operator $\mathbf{P}(t_0, \tau)$, obtained within the Ulam approach [13], whose matrix elements are given by :

$$\mathbf{P}(t_0, \tau)_{ij} = \frac{m(B_i \cap \Phi_{t_0+\tau}^{-\tau}(B_j))}{m(B_i)} \quad (1)$$

where $m(A)$ is a measure assigned to the set A . In our case, it is proportional to the amount of fluid it contains, i.e. simply its area. A probabilistic interpretation of Eq. (1) is that $\mathbf{P}(t_0, \tau)_{ij}$ is the probability for a particle to reach the box B_j , under the condition that it started from a uniformly random position within box B_i . Other measures referring for example to heat or salt content could be implemented for future applications. Eq. (1) states that the flow from box B_i to box B_j is the fraction of the contents of B_i which is mapped into B_j . If a nonuniform distribution of some conserved tracer is initially released in the system such that $\{p_i(t_0), i = 1, \dots, N\}$ is the amount of such tracer in each box $\{B_i\}$ at the initial instant t_0 , the matrix $\mathbf{P}(t_0, \tau)$ gives the evolution of this distribution after a time τ as $p_j(t_0 + \tau) = \sum_{i=1}^N p_i(t_0) \mathbf{P}(t_0, \tau)_{ij}$. Writing the $\{p_i\}$ as row vectors:

$$p(t_0 + \tau) = p(t_0) \mathbf{P}(t_0, \tau).$$

The matrix $\mathbf{P}(t_0, \tau)$ is row-stochastic, i.e. it has non-negative elements and $\sum_{j=1}^N \mathbf{P}(t_0, \tau)_{ij} = 1$, but is column stochastic the flow $\mathbf{v}(\mathbf{x}, t)$ is in-compressible. The quantity $\sum_{i=1}^N \mathbf{P}(t_0, \tau)_{ij}$ measures the ratio of fluid present in box B_j after a time τ with respect to its initial content at time t_0 . This ratio will be unity when the matrix is doubly stochastic (in-compressible flow).

As a standard way to evaluate numerically $\mathbf{P}(t_0, \tau)$, we apply the Lagrangian map to a large number of particles released uniformly inside each of the boxes $\{B_i, i = 1, \dots, N\}$ (Fig. 2). The initial number of particles in each box (Ω_i), is a proxy of the amount of fluid it contains and should be proportional to its measure $m(B_i)$. Therefore, since we work with boxes of equal area, we seed the same number of particles in each box ($\Omega_i = \Omega \quad \forall i$). The number of particles transported from box B_i to box B_j gives an estimation of the flow among these boxes. A numerical approximation to Eq. (1) is:

$$\mathbf{P}(t_0, \tau)_{ij} \approx \frac{\text{number of particles from box } i \text{ to box } j}{\Omega}$$

Because of the time-dependence of the velocity field, the results of the Lagrangian simulations will depend on both the initial time t_0 and the duration of the simulation τ . Once these parameters are fixed, we can build a network described by a transport matrix $\mathbf{P}(t_0, \tau)$ that characterizes the connections among each pair of nodes from initial time t_0 to final time $t_0 + \tau$. We interpret $\mathbf{P}(t_0, \tau)$ as the adjacency matrix of a weighted and directed network, so that $\mathbf{P}(t_0, \tau)_{ij}$ is the weight of the link from node i to node j .

The network constructed in this way characterizes the final locations of all fluid elements a time τ after their release at time t_0 , but gives no information on particle

locations at intermediate times. Also, since each of the matrices $\mathbf{P}(t_0 + k\tau, \tau)$, for $k = 0, 1, \dots, n - 1$, where $n\tau$ is the total time elapsed, is a stochastic matrix, one can consider the discrete time Markov chain in which an initial vector giving occupation probabilities $p(t_0) = (p_1(t_0), \dots, p_N(t_0))$ for the different boxes is evolved in time as $p(t_n) = p(t_0) \mathbf{P}(t_0, \tau) \mathbf{P}(t_1, \tau) \dots \mathbf{P}(t_{n-1}, \tau)$, where $t_k = t_0 + k\tau$. This time evolution will not be exactly equal to the true evolution $p(t_n) = p(t_0) \mathbf{P}(t_0, n\tau)$, but a Markovian approximation to it in which the memory of the particle positions is lost after a time τ . The Markovian approximation may be reasonable in some circumstances and in fact, it has been successfully used in geophysical flow problems [14].

Apart from the Markov assumption, replacing the continuous flow system with a discrete network introduces discretization errors. Even if the integration is done accurately, the initial and final locations of the transported particles are only specified up to a precision Δ , given by the linear side of the boxes. This implies that our network approach does not display explicitly fluid structures smaller than the box length-scale Δ .

Given the temporal matrix, let us now formally define its aggregated counterpart. The elements of $\mathbf{P}(t_0, \tau)_{i,j}$ account for the number of tracers that can be found in node j at time $t_0 + \tau$, which departed from position i at time t_0 . One commonly used approximation when evaluating advection over different periods of fixed duration τ is the *aggregated* matrix. Within this approximation, the dependence of the transport matrix on the initial time t is neglected. In particular, given an ensemble of T transport matrices $\mathbf{P}(t_i, \tau)$ with $t_1 < \dots < t_T$, the transport matrix is defined element-wise as:

$$\hat{\mathbf{P}}_{i,j}^\tau := \frac{1}{T} \sum_{t=x}^T \mathbf{P}(t_x, \tau)_{i,j}. \quad (2)$$

Then, the fully time-dependent matrices are replaced with the aggregated matrix:

$$\mathbf{P}(t_0, \tau) \approx \hat{\mathbf{P}}^\tau \quad \forall t \in [t_1, t_T].$$

Dynamical community detection

The fact that marine currents are not isotropic generates some sea areas that are better connected than others. Therefore, we expect different causal relations between different patches, resulting in a stronger influence of some areas over others. In the graph representation paradigm, this corresponds to a community structure. We here investigate such mesoscale structure and compare the results of community detection on the temporal and on the aggregated graphs.

Community detection [15] is a commonly studied inference problem that consists in partitioning the nodes of a network into tightly and non-overlapping groups. Formally, for each node i , one wants to define a mapping $i \rightarrow \ell(i) \in \{1, \dots, k\}$, where k is the number of communities. A practical challenge in this setting is related to the complexity of the network structure that is weighted, directed, and temporal. We use a dynamical spectral clustering algorithm inspired by [16], adapted to weighted and directed graphs.

The core idea of spectral clustering is to represent each node of the network as a vector in a low dimensional space, using the eigenvectors of a suited graph matrix representation. The vectors can then be divided into groups with, for instance, *k-means* algorithm [17] of *expectation-maximization* [18], as we do in the following. For static, weighted and directed networks, [19] showed that, even in the sparse regime in which typically many spectral algorithms tend to fail, one can obtain this embedding computing the k largest eigenvalues of the weighted adjacency matrix, store them in the columns of an embedding matrix $X \in R^{N \times k}$ and interpret its rows as embedding vectors. We

use this method to obtain the communities from the aggregated (static) graph. For the temporal one, instead, we generalize building the following matrix $\mathbf{M} \in R^{NT \times NT}$:

$$\mathbf{M} = \begin{pmatrix} \mathbf{P}(t_0, \tau) & hI_N & 0 & \dots & 0 \\ hI_N & \mathbf{P}(t_1, \tau) & hI_N & \dots & 0 \\ 0 & hI_N & \mathbf{P}(t_2, \tau) & \dots & 0 \\ \vdots & \vdots & \vdots & \ddots & 0 \\ 0 & 0 & 0 & \dots & \mathbf{P}(t_T, \tau) \end{pmatrix}$$

where I_N is the diagonal matrix of size N and $h > 0$ is a regularization parameter that imposes that the community label of each node must change slowly across time. In our simulations we set this regularizer value to $h/p = 0.2$, where p is the sum of all entries of \mathbf{P} . Every row of this matrix, and consequently of its eigenvectors, is associated to a node at a given time instant. The derivation of \mathbf{M} can be obtained following the steps described in [16], computing the Hessian matrix of the naïve mean field free energy (instead of the Bethe free energy) related to the same Hamiltonian matrix.

On top of the flexibility that allows one to deal at once with weighted, directed, temporal and sparse graphs, a major advantage of this approach is that one can estimate the number of communities k in an unsupervised fashion. In fact, \mathbf{M} is non-Hermitian, hence its eigenvalues are generally complex. In a model-based approach, however, the largest of these eigenvalues, are associated to its expectation that is – by definition – supposed to be symmetric of rank k . Hence, the first k largest eigenvalues of \mathbf{M} are real and by identifying the position of the first complex eigenvalue one can also estimate the number of communities, a typically hard task to solve.

Ecological modeling

A general model for the population dynamics of marine organisms that are affected by ocean currents can be written in the form,

$$\partial_t \mathbf{n}(x, t) = f(\mathbf{n}(x, t), x) + T(\mathbf{n}(x, t), x, t),$$

where \mathbf{n} is a vector whose components are the fish populations at point x and time t , f encodes the local population dynamics within and between species and T encodes the transport by the currents.

The Lagrangian approach for modeling currents can be used as a backbone for modeling and simulating such marine environments as the dynamics of ideal tracers can be used as a proxy for real population transport. When the time between the different transport networks $[\mathbf{P}(t_1, \tau) \dots, \mathbf{P}(t_T, \tau)]$ is small compared to the time scale of local population dynamics the transport-reaction system can be decoupled and estimated as a two-step process

The two steps of the simulations are; (i) update the populations at each node according to the local population dynamics; (ii) redistribution of the populations proportionally with the mobility matrix of the given period.

Results

We here discuss the main results of our analysis of the global network properties, the community structure, and the population dynamics.

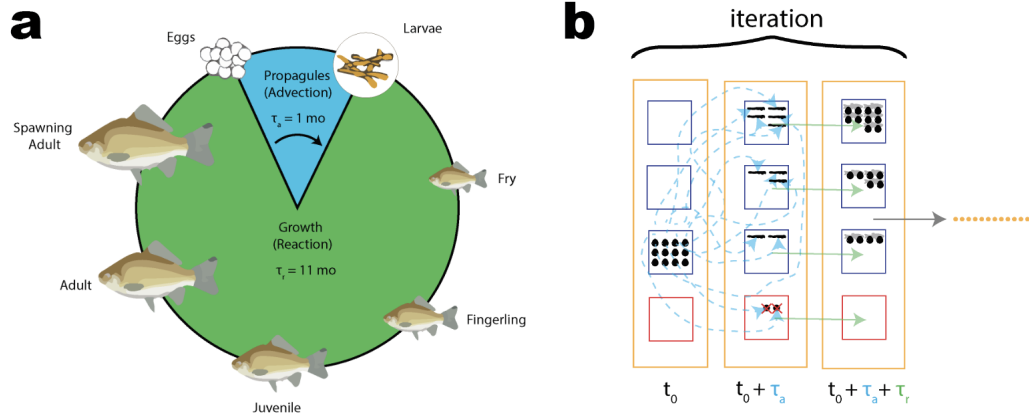


Figure 2. Conceptual illustration of advection-reaction model of fish. (a) Eggs are spawned as propagules until developed into larvae, are driven by the oceanic currents. The advective duration of one month fits the sampling time of the networks. During the growth period, the fish are less susceptible to oceanic current, allowing them to reproduce, in which the reactive duration of one year fits the total sampling duration. (b) In this model, we assume that fish eggs spawned in coastal regions. They follow the sea currents for a month (blue arrows) and settle in shallow water (purple boxes) as larvae, while those end up in deep sea (red boxes) cannot settle and die. The settled larvae will no longer be affected by the sea currents and they will undergo a growth cycle about 11 months (green arrows) and turn into adult fish. They then reproduce more eggs, beginning the next cycle.

Global network properties

Month by month network

One of our main objectives is to evaluate whether an aggregated matrix can be used as a proxy of the real fully time-dependent transport matrices. In Fig. 3, we compare the global properties of 12 month-by-month matrices and their corresponding aggregated matrix. The first fact that draws our attention is that the aggregated matrix is way denser in links than any of the month-by-month matrices. Indeed, in Fig. 3-(a) it is shown that the average degree of the aggregated matrix is always bigger than the average degree of any of the twelve month-by-month matrices. Furthermore, a temporal pattern that we associate with seasonality can be observed. Of course, this temporal pattern is destroyed using the aggregated matrix, which is time-independent. Similarly, in Fig. 3-(b) it is shown that the degree distribution is wider in the case of the aggregated matrix, meaning that one would expect an overall increase in the variability of the degrees. The fact that the degrees increase through the process of aggregation is expected since the degree can only increase or stay constant through this operation [Eq. (2)]. How much the degree of nodes increases depends on the variability of links across the different instances of transport matrices used to compute the aggregated matrix. The distribution of degrees in the aggregated matrix indicates that small degrees, similar to the ones observed in the month-by-month matrices, can occur with a similar probability as much larger degrees. Based on this observation, we assume that while the connections of some nodes change significantly between snapshots, the links of other nodes may remain relatively constant.

Apart from the connectivity, it is important to assess the effect of the aggregation of matrices on the weights of the links. Every node has an associated total outflow and

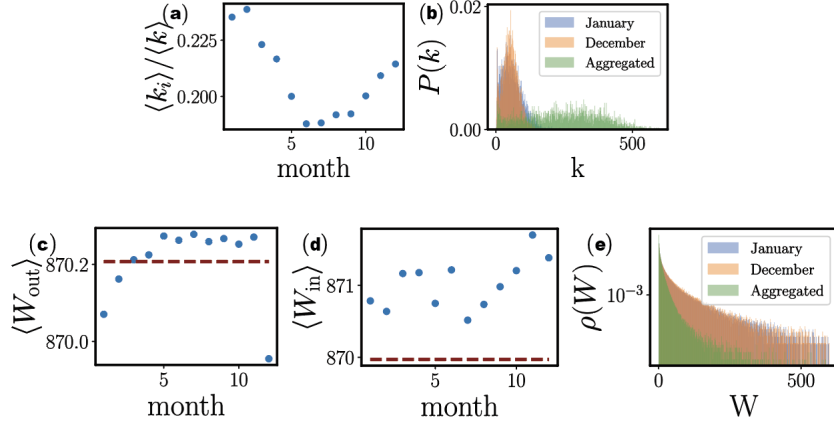


Figure 3. Degrees and weights of Aggregate transport matrix versus month-by-month transport matrices In (a), the average degree of the transport networks at different times $\langle k_i \rangle$ is divided by the average degree of the aggregated matrix ($\langle k \rangle \approx 250$). It can be observed that the average degree of the aggregated matrix is close to one order of magnitude bigger than the typical degree of the month-by-month matrices. Furthermore, a temporal pattern that we associate with seasonality can be observed. In (b), we provide a more detailed view by presenting the complete degree distribution for two months, as well as the aggregated mobility matrix. Both (a) and (b) clearly demonstrate significant discrepancies between the connectivity of the month-by-month transport matrices and the aggregated transport matrix. In (c), we show the average outflow for the month-by-month matrices (dots) fluctuate about the value obtained on the aggregated matrix (horizontal dashed line). Similarly, in (d) it can be observed that the average inflow is always bigger in the case of the month-by-month matrices. In (e), we show the distribution of weights for two months (January and December) together with the one corresponding to the aggregated matrix. Whereas the distributions for January and December are in agreement, the aggregated weights tend to be smaller.

inflow, defined respectively as

$$(W_{out})_i = \sum_j P(t_0, \tau)_{ij}, \quad (W_{in})_i = \sum_j P(t_0, \tau)_{ji}.$$

Since all nodes have a similar number of tracers at the initial time and all tracers must go somewhere, we expect that the outflow should be close to a constant. Indeed, in Fig. 3-(c) we show that the average outflow of transport matrices corresponding to different months agrees with the average outflow of the associated aggregated matrix. Since tracers can be accumulated in some destinations with many incomes, the average inflow does not need to be conserved. In Fig. 3-(d), it is shown that the inflow of the aggregated matrix tends to be smaller than in the time-dependent snapshots. This implies that inflows typically do not accumulate through matrix aggregation, as different snapshots often have varying destinations. Actually, all weights tend to be smaller in the aggregated matrix [Fig. 3-(e)]. Summing up the information provided through Figs. 3, the aggregated matrix tend to be more connected, but the number of tracers traveling through each link tends to be smaller. How these changes may affect the properties of the advection is a non-trivial question that we address in the remainder.

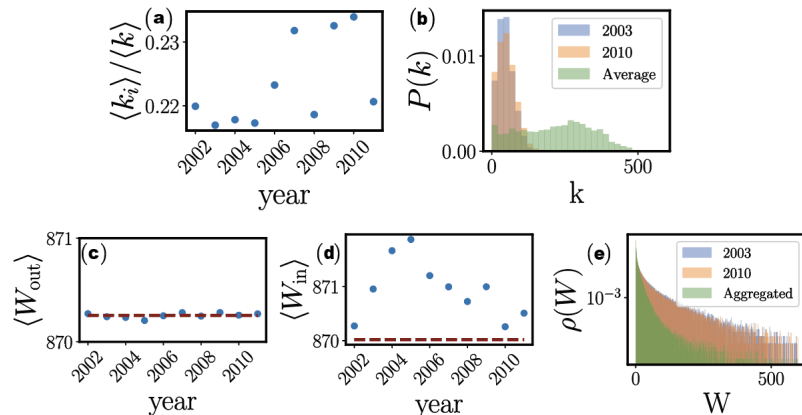


Figure 4. Degrees and weights of aggregate transport matrix versus year-by-year transport matrices In (a), the average degree of the transport networks at different times $\langle k_i \rangle$ is divided by the average degree of the aggregated matrix ($\langle k \rangle \approx 218$). It can be observed that the average degree of the aggregated matrix is close to one order of magnitude bigger than the typical degree of the year-by-year matrices. In (b), we provide a more detailed view by presenting the complete degree distribution for two years (2003 and 2010), as well as the aggregated mobility matrix. Both (a) and (b) clearly demonstrate significant discrepancies between the connectivity of the year-by-year transport matrices and the aggregated transport matrix. In (c), we show the average outflow for the year-by-year matrices (dots) fluctuate about the value obtained on the aggregated matrix (horizontal dashed line). Similarly, in (d) it can be observed that the average inflow is always bigger in the case of the year-by-year matrices. In (e), we show the distribution of weights for two years (2003 and 2010) together with the one corresponding to the aggregated matrix. Whereas the distributions for 2003 and 2010 agree within them, the weights for the aggregated matrix tend to be smaller.

Year-by-year network

In this section, we replicate the analysis conducted in section [Month by month network](#) using a different dataset, which pertains to transportation data from the same month but across ten different years. Through the plots in Fig. 4 we get a similar behavior to what was observed within the month-by-month dataset: whereas the connectivity increase through the aggregation of matrices, the weights per link tend to decrease. In the year-by-year dataset, we cannot appreciate coherent oscillations Fig. 4-(a) like the ones observed in the month-by-month dataset [Fig. 3-(a)], but rather random fluctuations.

Community structure

We aim to investigate how the global behaviors of oceanic flow are affected by seasons (short term) and climates (long term). We apply community detection to identify coherent regions in the sea, well mixed internally but with little exchange among them. In fig. 5a (i - iv), we plot the community structure in color code for 4 months and find that the community structure is slowly evolving over different months. In particular, the probability of the same node to be assigned to the same community in two successive time steps is approximately 0.8. We remark that some communities have a rather small size (most of them reflecting shallow oceanic regions such as continental shelves), and that there are especially some inter-seasonal variabilities.

On the other hand, the community structure of the same month across different

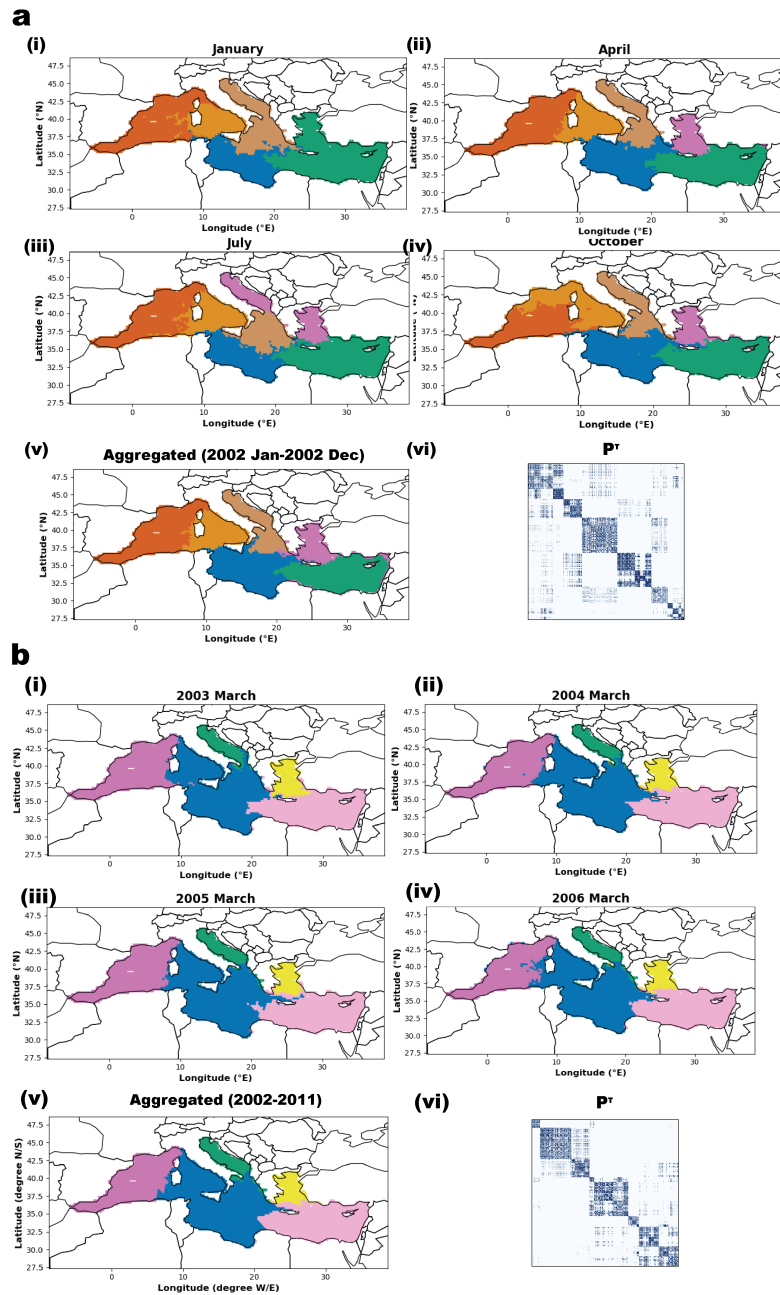


Figure 5. Communities of monthly mobility network. Community detection is performed on the transport networks and 6 communities (represented by the colors) are detected. (a.i-iv) four monthly transport networks (Jan, Apr, Jul and Oct in 2002) corresponding to four seasons are presented. Community structures change over the months, where most months deviate from the aggregated network community from Jan 2002 to Dec 2002 (a.v). (b.i-iv) four transport networks from July of 2003 to 2006. Community structures are similar for the same month across different years, over a 10 year period from 2002 to 2011 (b.v). The plots (vi) show the aggregated network on a basis so that nodes in the same community are close to one another.

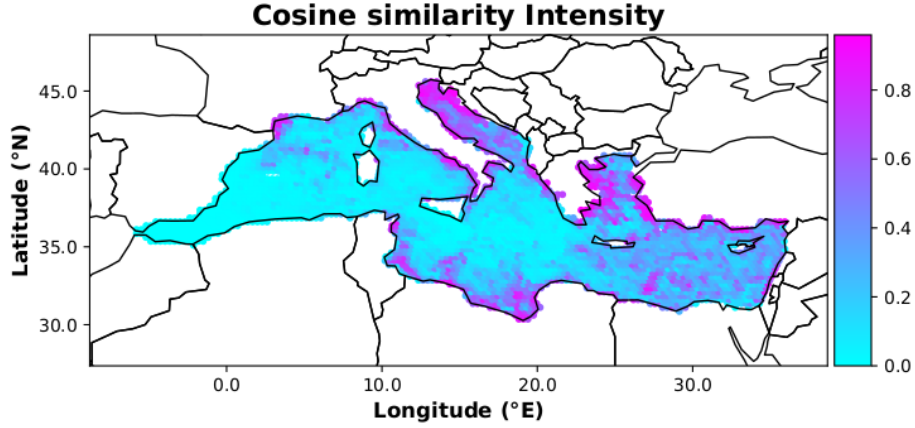


Figure 6. Synthetic modelling simulation. For each point of the map, we initialize the probability distribution to a Dirac delta and perform a simulation as per Equation (3) using the temporal transition matrices and the aggregated one. The color code shows the cosine similarity between the two final distributions and spans from 0 (cyan, in the Spain region) for different distributions to 1 (purple, Venice region) for equal distributions.

years is very stable (see fig. 5b (i - iv)). Indeed, the probability of being assigned to the same community in two successive time steps is larger than 0.9, suggesting that the main variability is due to a seasonal effect, as it was already commented in the previous section. To conclude, this implies that a dynamical process run on the network at the time-scale of months will be expected to have significant differences if one uses the temporal or the aggregated network. A less prominent role of time should be observed, instead, at the scale of years.

We now validate these claims modeling two types of dynamical processes on the network: one that is mainly theoretical in which diffusion is couple with time-dependent birth and death rates; the other that more reliably models an ecological system.

Modelling

Synthetic model

In this section we describe the effect of a transportation model with time-dependent birth and death rates. These functions couple with the network dynamics evidencing the importance of keeping the temporal dimension into account. Even though this model does not claim to be realistic, it shows the importance of keeping the temporal dimension into account whenever there is a dynamical process on the network coupling with its dynamics. We consider the following model, in which $p_i(t)$ denotes the probability of a particle to be in node i at time t .

$$p_i(t + \tau) = [\mathbf{P}(t, \tau)p]_i + (\lambda_t - \mu_t)p_i(t), \quad (3)$$

where λ_t, μ_t are the birth and death rates, respectively. We choose $\lambda_t = te^{-t/1.5}$ and $\mu_t = (T - t)e^{-(T-t)/1.5}$. This models the fact that in spring there is a blooming of births while in winter there is a higher mortality rate. As a consequence, the population size is not constant and is peaking around the month of April, while it is minimal towards the end of the year. Note that $\sum_t \lambda_t = \sum_t \mu_t$, implying that the population stays constant over the simulation time, even though the distribution are not constant.

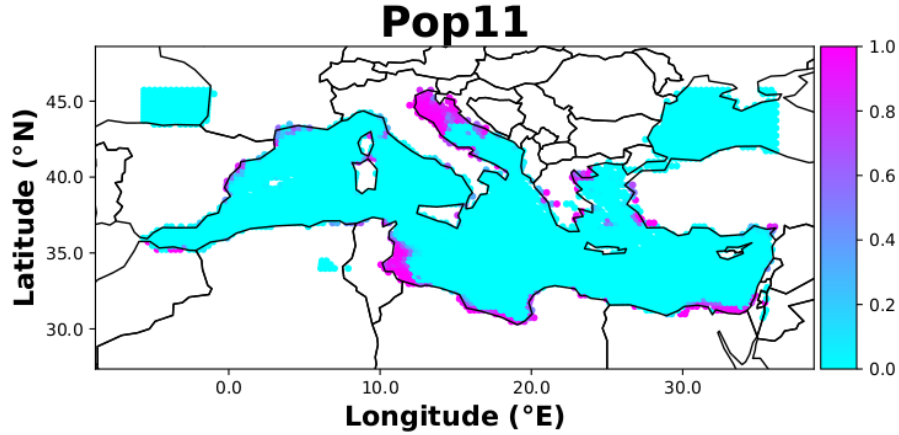


Figure 7. Result of the ecological modelling simulation in year 2011. Population of fish larvae for the year 2011 for $K = 1$ and $\nu = 1$.

To test the relevance of keeping the temporal dimension into account, we run several simulations: for each of them we set an initial distribution fully concentrated into a single node of the graph. We then run the diffusive process in two different ways: one in which at each time step we use the transition matrix of that time; the other in which we use the aggregated one. We then compare the resulting distributions in terms of cosine similarity.¹ Figure 6 shows in color code the obtained cosine similarity for each initialization points, evidencing that in some regions considerable discrepancies between the two models are observed. On the opposite – and coherently with the community detection analysis – other regions, such as the Adriatic sea, show a much larger agreement.

Ecological modeling

Our two-step simulation scheme is a good representation for the dynamics of some fish larvae [20]. After hatching, fish larvae enter a phase called the pelagic larval stage, where they spend a variable amount of time drifting with ocean currents until they settle in a region [see sketch in 2-(a)]. We illustrate our two-step approach for modeling ecological systems affected by currents through a simplified model for the population of fish larvae. In our model fish can only settle and lay eggs in shallow water for which we define as depths of less than 100m we refer to these nodes as shallow water nodes (SWN). After hatching larvae will drift along the currents for 1 month and settle if their location corresponds to SWN, or otherwise they die. The new population of eggs in each node then updates according to a logistic growth model

$$n_i(t) = \frac{K n_i(t-1)}{n(t-1) + (K - n_i(t-1))e^{-\nu\tau}} \quad (4)$$

where K is the capacity, and ν is the growth rate which we assume to be the same for all SWN. We simulate the model in the Mediterranean Sea sequentially for the months of July over the years 2002-2011. We initialize the larvae population uniformly on the shallow water nodes and use the first years 2002-2006 as a thermalization period.

The interplay of bathymetry landscape and currents shape the spatial distribution of the population to qualitatively similar population distribution of larvae.

¹The cosine similarity between two vectors is defined as $s(x, y) = \frac{x^T y}{\|x\|_2 \|y\|_2}$.

Particularly We see that the Adriatic sea and the Tunisian continental shelf regions have high populations. The population distribution in the SWN of the two regions are presented in Figure 7 for year 2011. In this preliminary analysis we observe low variability in the population distribution in the two regions over the years, but a general spatial heterogeneity from year to year that is driven by the currents.

Discussion

In this report we studied marine current flows with network theory tools analyzing in particular the role played by the time component of the network evolution. A typical approach consists in fact to neglect this dimension [9] and we investigated the consequences of this approximations under many different angles.

The analysis of the global properties of the transport networks reveals that the aggregated matrix has a higher number of links with relatively smaller weights per link, in comparison to the time-dependent snapshots and it thus corresponds to a more homogeneous distribution over space. In terms of simulation, we saw that a dynamical model with an explicit temporal dependence leads to a more homogeneously final distribution when adopting the aggregated network instead of the time-dependent one. On top of this “averaging” property, induced by the changes in connectivity, we also verified that the connections between nodes tend to vary among the different snapshots. These variations are observed at the local network structure, at a mesoscale community level, and are reflected in the output of the simulations as well. The time dependence of communities is easily observable when looking at the network across months, but is not so evident when looking at its evolution across years. We explain this difference between the across-month and across-year evolution as a consequence of seasonality. This result suggests that neglecting the time dependence of transport matrices could be a reasonable approximation depending on the specific time windows under consideration: a proper description of within-a-year transport phenomena will require the full time-dependent transport matrices in order to capture oscillations due to seasonality. The seasonal change of oceanic flow pattern is in accordance with previous studies [21]. Conversely, transport spanning multiple years can potentially be described adequately using aggregated time-independent matrices. Other studies provide evidence that there is no coherent trend in the Meridional Overturning Circulation due to climate change in small time scales [22]. In our case, the Mediterranean Sea is even more isolated than the Atlantic Ocean, so the variation due to short-term climate is minimal compared to seasonal effects.

We point out, however, that in all cases the aggregated matrix is denser, hence it tends to induce an artificial averaging effect. This effect has already been observed in epidemiological modeling, in which the larger degree artificially speeds up the spreading of an infectious disease [23]. The approach proposed in [23] to deal with this problem is to generate matrices that identify and preserve the most relevant ties of a temporal network without affecting the degree distribution.

This analysis evidenced the importance of the time component of the network describing marine flows. we acknowledge that these results are preliminary, since the dynamics of the network can be better captured by observed field and satellite data. Also, a realistic ecological model would require more complex considerations. Nevertheless, here we present a feasible framework combining oceanic transport network and ecological modeling which can already capture many important characteristics of real population dynamics. This encourages more work in the future as marine ecology has many determinants that interact in a complex way. The role of the temporal structure in more realistic scenarios can then be envisioned as a natural continuation of this work.

Acknowledgments

This work is the output of the Complexity72h workshop, held at IFISC in Palma de Mallorca, Spain, 26-30 June 2023 complexity72h.com. LD acknowledges the support from Fondation Botnar and from the Lagrange project of Fondazione CRT. Partial financial support has been received from the Agencia Estatal de Investigación and Fondo Europeo de Desarrollo Regional (FEDER, UE) under project APASOS (PID2021-122256NB-C21/PID2021-122256NB-C22), the María de Maeztu project CEX2021-001164-M, funded by the MCIN/AEI/10.13039/501100011033, and the Conselleria d'Educació, Universitat i Recerca of the Balearic Islands (Grant FPI FPI.006.2020).

References

1. P. V. R. Snelgrove, “The importance of marine sediment biodiversity in ecosystem processes,” *Ambio*, vol. 26, no. 8, pp. 578–583, 1997. [Online]. Available: <http://www.jstor.org/stable/4314672>
2. P. Koundouri and A. Giannouli, “Blue growth and economics,” *Frontiers in Marine Science*, vol. 2, 2015. [Online]. Available: <https://www.frontiersin.org/articles/10.3389/fmars.2015.00094>
3. J. F. de Moura, E. M. Roges, R. L. de Souza, S. Siciliano, and D. dos Prazeres Rodrigues, “Marine environment and public health,” in *Biodiversity Conservation and Utilization in a Diverse World*, G. A. Lameed, Ed. Rijeka: IntechOpen, 2012, ch. 11. [Online]. Available: <https://doi.org/10.5772/48412>
4. S. C. Doney, M. Ruckelshaus, J. Emmett Duffy, J. P. Barry, F. Chan, C. A. English, H. M. Galindo, J. M. Grebmeier, A. B. Hollowed, N. Knowlton, J. Polovina, N. N. Rabalais, W. J. Sydeman, and L. D. Talley, “Climate change impacts on marine ecosystems,” *Annual Review of Marine Science*, vol. 4, no. 1, pp. 11–37, 2012, pMID: 22457967. [Online]. Available: <https://doi.org/10.1146/annurev-marine-041911-111611>
5. R. I. Perry, R. E. Ommer, E. H. Allison, M. Badjeck, M. Barange, L. Hamilton, A. Jarre, R. A. Quiñones, and U. R. Sumaila, “221Chapter 8 Interactions between changes in marine ecosystems and human communities,” in *Marine Ecosystems and Global Change*. Oxford University Press, 02 2010. [Online]. Available: <https://doi.org/10.1093/acprof:oso/9780199558025.003.0008>
6. E. Villarino, J. R. Watson, B. Jönsson, J. M. Gasol, G. Salazar, S. G. Acinas, M. Estrada, R. Massana, R. Logares, C. R. Giner, M. C. Pernice, M. P. Olivar, L. Citores, J. Corell, N. Rodríguez-Ezpeleta, J. L. Acuña, A. Molina-Ramírez, J. I. González-Gordillo, A. Cózar, E. Martí, J. A. Cuesta, S. Agustí, E. Fraile-Nuez, C. M. Duarte, X. Irigoien, and G. Chust, “Large-scale ocean connectivity and planktonic body size,” *Nature Communications*, vol. 9, no. 1, p. 142, Jan 2018. [Online]. Available: <https://doi.org/10.1038/s41467-017-02535-8>
7. G. Coppini, E. Clementi, G. Cossarini, G. Korres, M. Drudi, A. Aydogdu, G. Bolzon, R. Escudier, L. Feudale, A. C. Goglio, A. Grandi, P. Lazzari, R. Lecci, S. Masina, N. Pinardi, J. Pistoia, S. Salon, M. Ravdas, A. Teruzzi, and A. Zacharioudaki, “The copernicus marine service ocean forecasting system for the mediterranean sea: 2015-2021 achievements and future perspectives,” *Mar.* 2022. [Online]. Available: <https://doi.org/10.5194/egusphere-egu22-12460>

-
8. T. Legrand, A. Chenuil, E. Ser-Giacomi, S. Arnaud-Haond, N. Bierne, and V. Rossi, “Spatial coalescent connectivity through multi-generation dispersal modelling predicts gene flow across marine phyla,” *Nature Communications*, vol. 13, no. 1, Oct. 2022. [Online]. Available: <https://doi.org/10.1038/s41467-022-33499-z>
 9. E. Ser-Giacomi, V. Rossi, C. López, and E. Hernández-García, “Flow networks: A characterization of geophysical fluid transport,” *Chaos: An Interdisciplinary Journal of Nonlinear Science*, vol. 25, no. 3, p. 036404, Mar. 2015. [Online]. Available: <https://doi.org/10.1063/1.4908231>
 10. G. Rossetti and R. Cazabet, “Community discovery in dynamic networks: a survey,” *ACM computing surveys (CSUR)*, vol. 51, no. 2, pp. 1–37, 2018.
 11. P. Oddo, M. Adani, N. Pinardi, C. Fratianni, M. Tonani, and D. Pettenuzzo, “A nested atlantic-mediterranean sea general circulation model for operational forecasting,” *Ocean Science*, vol. 5, no. 4, pp. 461–473, Oct. 2009. [Online]. Available: <https://doi.org/10.5194/os-5-461-2009>
 12. R. Courant, K. Friedrichs, and H. Lewy, “Über die partiellen differenzgleichungen der mathematischen physik,” *Mathematische Annalen*, vol. 100, no. 1, pp. 32–74, Dec. 1928. [Online]. Available: <https://doi.org/10.1007/bf01448839>
 13. G. Froyland, K. Padberg, M. H. England, and A. M. Treguier, “Detection of coherent oceanic structures via transfer operators,” *Physical Review Letters*, vol. 98, no. 22, May 2007. [Online]. Available: <https://doi.org/10.1103/physrevlett.98.224503>
 14. M. Dellnitz, G. Froyland, C. Horenkamp, K. Padberg-Gehle, and A. S. Gupta, “Seasonal variability of the subpolar gyres in the southern ocean: a numerical investigation based on transfer operators,” *Nonlinear Processes in Geophysics*, vol. 16, no. 6, pp. 655–663, Dec. 2009. [Online]. Available: <https://doi.org/10.5194/npg-16-655-2009>
 15. S. Fortunato and D. Hric, “Community detection in networks: A user guide,” *Physics reports*, vol. 659, pp. 1–44, 2016.
 16. L. Dall’Amico, R. Couillet, and N. Tremblay, “Community detection in sparse time-evolving graphs with a dynamical bethe-hessian,” *Advances in Neural Information Processing Systems*, vol. 33, 2020.
 17. S. Lloyd, “Least squares quantization in pcm,” *IEEE transactions on information theory*, vol. 28, no. 2, pp. 129–137, 1982.
 18. A. P. Dempster, N. M. Laird, and D. B. Rubin, “Maximum likelihood from incomplete data via the em algorithm,” *Journal of the royal statistical society: series B (methodological)*, vol. 39, no. 1, pp. 1–22, 1977.
 19. S. Coste and L. Stephan, “A simpler spectral approach for clustering in directed networks,” *arXiv preprint arXiv:2102.03188*, 2021.
 20. E. A. Treml, P. N. Halpin, D. L. Urban, and L. F. Pratson, “Modeling population connectivity by ocean currents, a graph-theoretic approach for marine conservation,” *Landscape Ecology*, vol. 23, pp. 19–36, 2008.
 21. J. Callies, R. Ferrari, J. M. Klymak, and J. Gula, “Seasonality in submesoscale turbulence,” *Nature Communications*, vol. 6, no. 1, Apr. 2015. [Online]. Available: <https://doi.org/10.1038/ncomms7862>

-
22. C. Garcia-Soto, L. Cheng, L. Caesar, S. Schmidtko, E. B. Jewett, A. Cheripka, I. Rigor, A. Caballero, S. Chiba, J. C. Báez, T. Zielinski, and J. P. Abraham, “An overview of ocean climate change indicators: Sea surface temperature, ocean heat content, ocean pH, dissolved oxygen concentration, arctic sea ice extent, thickness and volume, sea level and strength of the AMOC (atlantic meridional overturning circulation),” *Frontiers in Marine Science*, vol. 8, Sep. 2021. [Online]. Available: <https://doi.org/10.3389/fmars.2021.642372>
 23. T. Kobayashi, T. Takaguchi, and A. Barrat, “The structured backbone of temporal social ties,” *Nature communications*, vol. 10, no. 1, p. 220, 2019.